Phonon Raman study of the $NdBa_2Cu_3O_y$-$Nd_2Ba_1Cu_3O_y$ system

M. F. Limonov,* E. A. Goodilin, X. Yao, S. Tajima, and Y. Shiohara
Superconductivity Research Laboratory, International Superconductivity Technology Center, 10-13, Shinonome 1-Chome, Koto-ku, Tokyo, 135 Japan

Yu. E. Kitaev
A. F. Ioffe Physical-Technical Institute, 194021 St. Petersburg, Russia
(Received 11 December 1997; revised manuscript received 2 March 1998)

We have investigated Raman-scattering spectra of $Nd_{1+x}Ba_{2-x}Cu_3O_y$ solid solutions with $x=0.0-0.9$. For two compositions of $x=0$ and $x=0.85$, the Raman spectra were measured using detwinned or twinned single crystals. The observed spectra of $Nd_{1.85}Ba_{1.15}Cu_3O_z$ can be interpreted properly if an approximate structure with a doubled unit cell is assumed. Two x-dependent phase transitions in $Nd_{1+x}Ba_{2-x}Cu_3O_y$ solid solutions were analyzed by a joint study of Raman scattering and x-ray diffraction. The first transition at $x\approx 0.3$ is connected mainly with disordering of oxygen atoms, while the second transformation at $x\approx 0.6$ is induced by the Nd^{3+} and Ba^{2+} ions ordering in the structure.
[S0163-1829(98)06141-4]

I. INTRODUCTION

The Nd-Ba-Cu-O system is one of the most promising for development of high-temperature superconductors, because $NdBa_2Cu_3O_y$ demonstrates higher T_c in comparison with $YBa_2Cu_3O_y$ and enhanced vortex pinning, which results in the high critical current density and the high irreversibility field.[1,2] These phenomena are expected to be closely related to fundamental properties of the system, particularly similar sizes of Ba^{2+} and Nd^{3+} ions and a wide range of the $Nd_{1+x}Ba_{2-x}Cu_3O_y$ solid solutions. It is believable that existence of the solid solution may play an important role in explanation of the advanced physical properties.[1–6] According to Refs. 3–6, the $Nd_{1+x}Ba_{2-x}Cu_3O_y$ stability region is limited by $0-0.04\leqslant x\leqslant 0.6-0.7$; however, it has been found recently to be more extended: $0\leqslant x\leqslant 1.0$.[7–9] The most significant aspect to discuss hereinafter is connected with a possibility of local and/or long-range ordering of the heavy atoms (Nd and Ba) and its interrelation with the oxygen ordering in all the existing solid solutions. It has not been investigated properly yet, although at least two scenarios connected with the ordering were suggested to explain, for example, the anomalous peak effect for $NdBa_2Cu_3O_y$ single crystals[2] and the $Nd_2Ba_1Cu_3O_y$ phase superstructure.[7] The recently obtained $Nd_2Ba_1Cu_3O_y$ phase exhibits doubling of the parent sublattice in the a- and c-axis directions because of the Nd^{3+} and Ba^{2+} cations exchange between their crystallographic sites. It was found by the electron diffraction and x-ray diffraction Rietveld refinement that the $Nd_2Ba_1Cu_3O_7$ crystal symmetry is described in a frame of the $C_{2v}^{14}(B2mm)$ space group with a single face-centered-orthorhombic Bravais lattice[7] (Fig. 1), as confirmed in Refs. 10 and 11. This phase has been also detected by transmission electron microscope and microenergy dispersive x-ray spectroscopy investigations of single crystals with the so-called anomalous peak effect caused by nanoscale compositional waves fluctuating between superconducting $NdBa_2Cu_3O_y$ and nonsuperconducting $Nd_2Ba_1Cu_3O_y$ regions of about several tens of nanometers.[2] It should be underscored that the crystals were high quality and contamination free; consequently, the peak effect can be related to the Nd-Ba-Cu-O system peculiarities, such as the $Nd_{1+x}Ba_{2-x}Cu_3O_y$ solution demixing into two terminal compounds $NdBa_2Cu_3O_y$ and $Nd_2Ba_1Cu_3O_y$.[2] From this point of view the $Nd_2Ba_1Cu_3O_y$ phase could be considered as a macroscopically separated part of such a system. A careful investigation of $Nd_2Ba_1Cu_3O_y$ as well as, more generally, the $Nd_{1+x}Ba_{2-x}Cu_3O_y$ solid solution at different x, can give much information to elucidate the pinning center formation mechanisms and other superconducting properties of Nd-based superconductors.

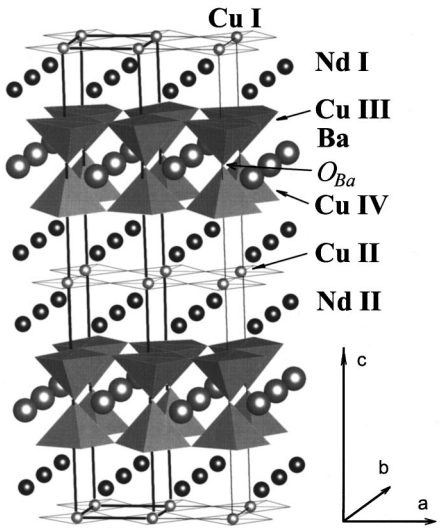

FIG. 1. Crystal structure of $Nd_2BaCu_3O_7$. The crystallographic unit cell of $2X$-$2Z$ structure is shown by thin lines; the primitive unit cell of the X-$2Z$ structure is drawn by thick solid lines. Atoms are labeled as in Table II.

The Raman spectroscopy is widely used for investigation of lattice dynamics of high-temperature superconductors (for example, see reviews in Refs. 12 and 13). The Raman-scattering spectra (RSS) of the $NdBa_2Cu_3O_y$ compound were obtained in ceramics[14] and twinned crystals;[15] however, for a complete interpretation of RSS it is required to measure RSS of twin-free crystals.[16,17] On the other hand, to our knowledge, no Raman study of another terminal solid solution $Nd_2Ba_1Cu_3O_y$ has been reported yet and no systematic study of RSS over the whole composition range x has been performed until now in the $Nd_{1+x}Ba_{2-x}Cu_3O_y$ system. In this work, we investigated the RSS of the detwinned $NdBa_2Cu_3O_y$ crystal and the twinned $Nd_{1.85}Ba_{1.15}Cu_3O_y$ crystal as well as polycrystalline $Nd_{1+x}Ba_{2-x}Cu_3O_z$ materials with $0.05 \leqslant x \leqslant 0.9$ in order to get more structural information via the lattice vibrations study. To interpret Raman spectra of the newly obtained $Nd_{1.85}Ba_{1.15}Cu_3O_y$ single crystals[9,18] we performed a group-theory analysis (GTA) for the $Nd_2Ba_1Cu_3O_7$ structure using the method of induced band representations of space groups.[19] This method was found to be highly effective for a wide variety of crystals with a large number of atoms per primitive cell,[13,20] such as Y-based[21] and Bi-based[22] high-T_c compounds. The following interpretation of the RSS enabled us to describe the RSS of $Nd_{1+x}Ba_{2-x}Cu_3O_y$ over the whole composition range (x). The observed spectral changes are consistent with the suggested models of phase transitions at $x \approx 0.3$ and $x \approx 0.6$ and the experimental data on x-ray diffraction (XRD).

II. EXPERIMENTS

The ceramic samples of $Nd_{1+x}Ba_{2-x}Cu_3O_y$ solid solutions were obtained by sintering at 1010 °C in air an oxide mixture prepared from CuO, $Ba(NO_3)_2$, and Nd_2O_3 powders as in Ref. 7. All the samples were synthesized under the same conditions to ensure that the composition x is the only parameter responsible for structural changes.[9] The two terminal compositions ($x=0.05$ and $x=0.9$) were chosen as close as possible to the homogeneity range limits to avoid impurities at the preparation temperature. Single crystals of the $Nd_{1+x}Ba_{2-x}Cu_3O_y$ solid solutions were grown by the ''top-seeded-solution-growth'' crystal pulling technique from the $Nd_{0.921}Ba_3Cu_{14.5}O_y$ flux.[18] The $NdBa_2Cu_3O_y$ single crystal was grown by the modified ''top-seeded-solution-growth'' method using the automated pulling equipment.[24]

In order to confirm preparation of the $Nd_{1+x}Ba_{2-x}Cu_3O_y$ solid solution, ceramic samples with different x values were analyzed using the XRD technique. No secondary phase was found in the samples either after quenching or oxygenation, the 113 peak near $2\Theta = 40°$ was single; therefore the samples cannot be considered as a mechanical mixture of different phases or solid solutions with different compositions. Additionally, the limit $x=0.9$ solid solution was quantitatively analyzed by the JEOL Superprobe 8600 series electron-probe microanalysis analyzer (accelerated voltage of 15 kV, a $NdBa_2Cu_3O_y$ single crystal used as a standard specimen), and the average composition of 20–30 particles randomly selected in this sample was confirmed to be $Nd_{1.94(3)}Ba_{1.10(4)}Cu_{2.97(5)}O_y$. The oxygenation procedure of the samples was performed by annealing in the oxygen atmosphere at 400 °C to be sure that the temperature is below the kinetically allowed region of the microscopic phase segregation reported in literature.[2] The linewidth of XRD reflexes (particularly, a single $hkl=113$ line) was found to be similar to that of the silicon powder, which was admixed with our samples as an internal standard for the lattice constant measurement. It suggests that the contribution of nanoscale distortions, which have to occur in the case of microscopic phase separation, is minimal and the samples are uniform. The detailed preparation conditions, x-ray diffraction, oxygen content analysis, and properties of $Nd_{1+x}Ba_{2-x}Cu_3O_y$ ceramics are discussed in a separate paper.[23] The structure analysis of the ceramic samples was performed as described in Ref. 9. The peak assignment and detailed experimental XRD data for the $x=0.9$ solid solution at room and elevated temperatures (1000 °C) are given in Ref. 10.

The as-grown crystals were characterized by the Laue XRD method. A fourfold symmetry was observed for the bottom facet, indicating the *ab* plane orientation of this face. The XRD for a powder obtained by crushing the crystals did not detect any secondary phase or flux inclusions. All the XRD peaks were indexed well and the lattice constant calculation gives only small deviations for 20–25 reflexes: $a=2\times3.8841(6)$, $b=3.8635(4)$, $c=2\times11.585(2)$.[18] The superstructure was confirmed by the selected area electron diffraction.[10] The chemical composition of the $Nd_{1.85}Ba_{1.15}Cu_3O_y$ crystal was proved by the quantitative EPMA line analysis with 340 successive 4-μm steps over the distance of 1360 μm ($Nd_{1.84(2)}Ba_{1.17(2)}Cu_{2.99(3)}O_y$). In contrast to the superconducting $NdBa_2Cu_3O_y$ ($y\sim7$) single crystal with a transition temperature about 95 K, the $Nd_{1.85}Ba_{1.15}Cu_3O_y$ ($y\sim7$) single crystal was found to be insulating with resistivity of about 200 Ω cm at room temperature and about 350 kΩ cm at 77 K.

The $NdBa_2Cu_3O_y$ crystal was detwinned[25] by applying a uniaxial pressure of about 10 MPa when cooling from 700° to 490 °C in oxygen. The $Nd_{1.85}Ba_{1.15}Cu_3O_y$ crystal was not detwinned since twinning in this material is connected with the crystal growth mechanism and detwinning techniques have not been developed yet.[10]

The RSS were measured at the room temperature using a triple spectrometer T64000 Jobin-Ivon equipped with a liquid-nitrogen-cooled change coupled device detector. The typical spectral resolution was 3 cm^{-1}. The 514.5-nm line of Ar-Kr laser was used for the excitation with a power density of 1 W/cm^2 on the sample surface. The pseudobackscattering configuration was adopted. In the case of the $NdBa_2Cu_3O_y$ crystal, the *xx*- and *yy*-polarized RSS were obtained from the same regions on the mirrorlike surface of crystals. As for the *zz* polarizations, the RSS taken from the *ac* and *bc* surfaces were nearly the same. The experimental errors in frequencies and widths of the Raman lines, which will be indicated by bars in the figures, were predominantly governed by the spectral slit, the shift of Raman-scale zero, etc., while the curve-fitting procedure introduced minor errors.

III. RESULTS AND DISCUSSIONS

A. Raman-scattering spectra and phonon mode assignment

The RSS of the oxygen-annealed twin-free $NdBa_2Cu_3O_y$ single crystal ($y\sim7$, T_c about 95 K) are shown in Fig. 2(a).

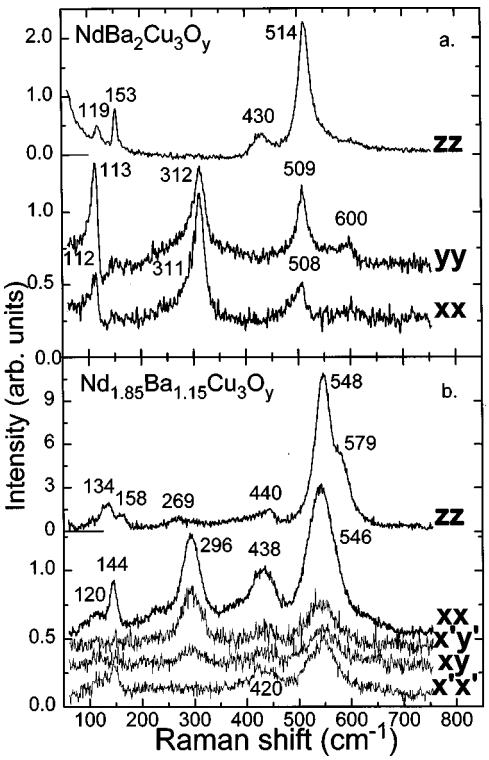

FIG. 2. Polarized Raman spectra of $NdBa_2Cu_3O_y$ detwinned single crystals ($y \approx 7$) and $Nd_{1.85}Ba_{1.15}Cu_3O_y$ single crystals at the room temperature.

The observed RSS are similar to the well-known spectra of the isostructural $YBa_2Cu_3O_y$ crystals[12,13] and in good agreement with the reported RSS of $NdBa_2Cu_3O_y$ ceramics and twinned crystals.[14,15] According to GTA for the orthorhombic $NdBa_2Cu_3O_7$ structure with the space group D_{2h}^1, the $5A_g(xx,yy,zz)+5B_{2g}(xz)+5B_{3g}(yz)$ vibrations are Raman active with the A_g mode lines being the most intense ones. The observed line frequencies are listed in Table I. The A_g vibrations are induced by the z displacements of Ba atoms (ν_1 mode), Cu atoms (ν_3 mode), out-of-phase and in-phase displacements of oxygen in the CuO_2 plane (ν_5 and ν_7 modes), and the apical oxygen atoms (ν_9 mode). This mode assignment is well established.[12,14,15]

In the perfect $NdBa_2Cu_3O_7$ structure, the Nd, Cu1, O_{Cu1} atoms (the atoms are labeled as in Ref. 13) are located at high-symmetry positions. Therefore, they contribute to the IR-active odd-symmetry modes that are not Raman active. However, oxygen deficiency in the $NdBa_2Cu_3O_y$ structure results in violation of the selection rules. In particular, the vibrations of Cu1 and O_{Cu1} atoms from chains become Raman active and an additional ν_{10} line appears in the RSS for *yy* and *zz* polarizations. This mode is connected with O_{Cu1} vibrations along the chains (B_{2u} symmetry in the exact $NdBa_2Cu_3O_7$ structure).

In the RSS presented in Fig. 2(a) one can see an effect of a strong interaction between phonons and anisotropic electronic background, resulting in different frequencies of Raman lines in different polarizations for the same mode. The most pronounced effect is observed for ν_1 and ν_9 vibrations, i.e., the line frequencies in the *xx* and *yy* spectra with strong electronic background are smaller than in the *zz* spectrum with almost negligible background. A similar effect was reported for $YBa_2Cu_3O_y$.[16,17] One can see also a significant difference in line intensities in the *xx* and *yy* spectra, which is the evidence that the crystal is properly detwinned.

Next, in Fig. 2(b), the RSS of the $Nd_{1.85}Ba_{1.15}Cu_3O_y$ single crystal are shown in *xx*, $x'y'$, $x'x'$, and *zz* polarizations. (The x' and y' axes are 45° rotated along the z axis with respect to the x and y.) No significant difference between the RSS in the *xx* and *yy* polarizations was detected in this orthorhombic crystal probably because of the twinning.[10] There are six pronounced lines in the *zz* polarization, and

TABLE I. Frequencies (cm^{-1}), polarizations, and assignments of observed Raman-active modes in $NdBa_2Cu_3O_y$ detwinned single crystals, $Nd_{1.85}Ba_{1.15}Cu_3O_y$ single crystals, and $Nd_{1.9}Ba_{1.1}Cu_3O_7$ ceramic samples at room temperature. All samples are oxygen annealed.

$NdBa_2Cu_3O_y$				$Nd_{1.85}Ba_{1.15}Cu_3O_y$		$Nd_{1.9}Ba_{1.1}Cu_3O_7$	
	112	*xx*		~120	*xx*		
ν_1	113	*yy*	Ba	~120	*yy*	134	Ba
	119	*zz*		134	*zz*		
ν_2				144	*xx,yy*		Ba/Cu/Nd
ν_3	153	*zz*	Cu	158	*zz*	~155	Cu
ν_4				269	*zz*	~270	Nd
	311	*xx*		296	*xx*		
ν_5			O_{CuIII}, O_{CuIV}	296	$x'y'$	295	O_{CuIII}, O_{CuIV}
	312	*yy*		296	*yy*		
ν_6				420	$x'x'$	420	O
				438	*xx,yy*		
ν_7	430	*zz*	O_{CuIII}, O_{CuIV}	440	*zz*	443	O_{CuIII}, O_{CuIV}
ν_8						524	O
	508	*xx*		546	*xx*		
ν_9	509	*yy*	O_{Ba}	546	*yy*	562	O_{Ba}
	514	*zz*		548	*zz*		
ν_{10}	600	*yy,zz*	O_{CuI}	579	*zz*		O_{CuI}

TABLE II. Atoms in the primitive cell of $Nd_2BaCu_3O_7$: exact and approximate symmetry structures.

Exact symmetry[a] $2X$-$2Z$ structure		Approximate symmetry X-$2Z$ structure		X-Z structure	
Atom and its site symmetry	Atom coordinates	Atom and its site symmetry	Atom coordinates	Atom and its site symmetry	Atom coordinates
Nd1(C_s)	$(0.253,\frac{1}{2},\pm0.076)$	NdI(C_{4v})	$(\frac{1}{2},\frac{1}{2},\pm0.076)$	NdI-II(C_{4v})	$(\frac{1}{2},\frac{1}{2},\pm0.152)$
Nd2(C_s)	$(0.243,\frac{1}{2},\pm0.4232)$	NdII(C_{4v})	$(\frac{1}{2},\frac{1}{2},\pm0.424)$		
Ba(C_s)	$(0.25,\frac{1}{2},\pm0.2593)$	Ba(C_{4v})	$(\frac{1}{2},\frac{1}{2},\pm0.259)$	Ba(D_{4h})	$(\frac{1}{2},\frac{1}{2},\frac{1}{2})$
O_1(C_s)	$(0.51,0,\pm0.252)$	O_{Ba}(C_{4v})	$(0,0,\pm0.252)$	O_{Ba}(D_{4h})	$(0,0,\frac{1}{2})$
Cu1(C_{2v})	(0.005,0,0)	CuI(D_{4h})	(0,0,0)	CuI-II(D_{4h})	(0,0,0)
Cu2(C_{2v})	$(-0.013,0,\frac{1}{2})$	CuII(D_{4h})	$(0,0,\frac{1}{2})$		
O4(C_{2v})	$(0.51,\frac{1}{2},0)$	O_{CuI}(D_{2h})	$(\frac{1}{2},0,0)$,		
O5(C_{2v})	$(0.05,\frac{1}{2},0)$		$(0,\frac{1}{2},0)$	$O_{CuI\text{-}II}$(D_{2h})	$(\frac{1}{2},0,0)$,
O8(C_{2v})	$(0.26,0,\frac{1}{2})$	O_{CuII}(D_{2h})	$(\frac{1}{2},0,\frac{1}{2})$,		$(0,\frac{1}{2},0)$
O9(C_{2v})	$(0.76,0,\frac{1}{2})$		$(0,\frac{1}{2},\frac{1}{2})$		
Cu3(C_s)	$(0.013,0,\pm0.162)$	CuIII(D_{4v})	$(0,0,\pm0.16)$	CuIII-IV(D_{4h})	$(0,0,\pm0.32)$
Cu4(C_s)	$(-0.016,0,\pm0.343)$	CuIV(D_{4v})	$(0,0,\pm0.34)$		
O2(C_s)	$(0.101,\frac{1}{2},\pm0.159)$	O_{CuIII}(C_{2v})	$(0,\frac{1}{2},\pm0.16)$,		
O6(C_s)	$(0.26,0,\pm0.159)$		$(\frac{1}{2},0,\pm0.16)$	$O_{CuIII\text{-}IV}$(C_{2v})	$(\frac{1}{2},0,\pm0.32)$,
O3(C_s)	$(0.25,0,\pm0.347)$	O_{CuIV}(C_{2v})	$(0,\frac{1}{2},\pm0.34)$,		$(0,\frac{1}{2},\pm0.32)$
O7(C_s)	$(0,\frac{1}{2},\pm0.348)$		$(\frac{1}{2},0,\pm0.34)$		

[a]We neglect small z shifts of O8 and O9 atoms (-0.032 and -0.028, respectively) from $z=\frac{1}{2}$ plane. In the crystallographic unit cell, all atoms have their translationally equivalent counterparts shifted by $(\frac{1}{2},0,\frac{1}{2})$ that do not enter into the primitive unit cell.

five of them (ν_1, ν_3, ν_7, ν_9, ν_{10}) originate from the $NdBa_2Cu_3O_y$ lattice vibrations, as listed in Table I.

According to Ref. 7, the $Nd_2Ba_1Cu_3O_7$ crystal lattice with the space group C_{2V}^{14} can be obtained from the basic $NdBa_2Cu_3O_7$ cell with translations $\mathbf{a}_{sub}$, $\mathbf{b}_{sub}$, and $\mathbf{c}_{sub}$ by imposing the superstructure with the orthogonal translation vectors $\mathbf{a}=2\mathbf{a}_{sub}$, $\mathbf{b}=\mathbf{b}_{sub}$, and $\mathbf{c}=2\mathbf{c}_{sub}$. In this paper we call this lattice the ''$2X$-$2Z$'' structure (see Fig. 1). The vectors **a**, **b**, and **c** are directed along the edges of the crystallographic unit cell. The primitive translations ($\mathbf{a}_1^{2X\text{-}2Z}$, $\mathbf{a}_2^{2X\text{-}2Z}$, $\mathbf{a}_3^{2X\text{-}2Z}$) are expressed in terms of **a**, **b**, **c** as $\mathbf{a}_1^{2X\text{-}2Z}=\frac{1}{2}(\mathbf{a}-\mathbf{c})$, $\mathbf{a}_2^{2X\text{-}2Z}=\mathbf{b}$, $\mathbf{a}_3^{2X\text{-}2Z}=\frac{1}{2}(\mathbf{a}+\mathbf{c})$. Therefore, the primitive unit cell is two times smaller than the crystallographic unit cell and the number of formula units of $Nd_2Ba_1Cu_3O_7$ per primitive cell is $Z=2$. The atom coordinates in terms of **a**, **b**, and **c** and their site symmetry in the primitive cell are given in Table II. According to the GTA (see Table III), the set of optical modes in the Brillouin-zone center is

$$\Gamma_{opt}=25\Gamma_1+10\Gamma_2+25\Gamma_3+15\Gamma_4 = 25A_1+10A_2+25B_2+15B_1. \quad (1)$$

Although 75 Raman-active modes are predicted, the number of observed phonon lines is much smaller. Most probably, some of the lattice distortions, leading to the lower C_{2V}^{14} symmetry, give only lines with negligible intensity or result in insignificant splitting of the lines. Therefore, to simplify the interpretation and establish the spectral line hierarchy on the base of the group-theory description, we assume two approximate structures with the D_{4h}^1 space group.

In the first approximation, we neglect all atomic modulations in the xz plane as shown in Table II. In this case, the crystal is described by the D_{4h}^1 structure with a primitive cell containing only one formula unit (X-Z model hereinafter) and the following primitive translations: $\mathbf{a}_1^{X\text{-}Z}=\mathbf{a}/2=\mathbf{a}_{sub}$, $\mathbf{a}_2^{X\text{-}Z}=\mathbf{b}=\mathbf{b}_{sub}$, $\mathbf{a}_3^{X\text{-}Z}=\mathbf{c}/2=\mathbf{c}_{sub}$ [a structure without additional (superstructural) ordering of cations or oxygen could be reflected by such a model]. In the second approximation, we consider the structure with a lower symmetry by introducing shifts of the BaO layers as presented also in Table II. In this case, the primitive cell becomes two times larger in z direction (two formula units per primitive cell) but the space group remains D_{4h}^1 with primitive translations: $\mathbf{a}_1^{X\text{-}2Z}=\mathbf{a}/2=\mathbf{a}_{sub}$, $\mathbf{a}_2^{X\text{-}2Z}=\mathbf{b}=\mathbf{b}_{sub}$, $\mathbf{a}_3^{X\text{-}2Z}=\mathbf{c}=2\mathbf{c}_{sub}$ (see Fig.

TABLE III. The correspondence between the modes for exact symmetry crystal and two approximate structures and Raman selection rules. Polarizations in capitals correspond to modes allowed in all three cases, those in small letters correspond to modes allowed both in the X-$2Z$ and $2X$-$2Z$ structures whereas polarizations in brackets correspond to modes allowed only in the $2X$-$2Z$ structure.

Approximate symmetry				Exact symmetry	
X-Z structure		X-$2Z$ structure		$2X$-$2Z$ structure	
Mode	Selection rules	Mode	Selection rules	Mode	Selection rules
$3A_{1g}$	*XX,YY,ZZ*	$3A_{1g}(3\Gamma_1^+)$	*XX,YY,ZZ*	$3A_1[3A_{1g}(3\Gamma_1^+)]$	*XX,YY,ZZ*
		$3A_{1g}(3Z_1^+)$	*xx,yy,zz*	$3A_1[3A_{1g}(3Z_1^+)]$	*xx,yy,zz*
$1B_{1g}$	*XX,YY*	$1B_{1g}(\Gamma_2^+)$	*XX,YY*	$1A_1[1B_{1g}(\Gamma_2^+)]$	*XX,YY,*[*zz*]
		$1B_{1g}(Z_2^+)$	*xx,yy*	$1A_1[1B_{1g}(Z_2^+)]$	*xx,yy,*[*zz*]
$4E_g$	*XZ,YZ*	$4E_g(4\Gamma_5^+)$	*XZ,YZ*	$4A_2[4E_g(4\Gamma_5^+)]$	*YZ*
				$4B_2[4E_g(4\Gamma_5^+)]$	*XZ*
		$4E_g(4Z_5^+)$	*xz,yz*	$4A_2[4E_g(4Z_5^+)]$	*yz*
				$4B_2[4E_g(4Z_5^+)]$	*xz*
$5A_{2u}$		$5A_{2u}(5\Gamma_3^-)$		$5B_2[5A_{2u}(5\Gamma_3^-)]$	[*xz*]
		$5A_{2u}(5Z_3^-)$		$5B_2[5A_{2u}(5Z_3^-)]$	[*xz*]
$2A_{2u}$		$2A_{2u}(2\Gamma_3^-)$		$2B_2[2A_{2u}(2\Gamma_3^-)]$	[*xz*]
		$2A_{1g}(2Z_1^+)$	*xx,yy,zz*	$2A_1[2A_{1g}(2Z_1^+)]$	*xx,yy,zz*
$2B_{2u}$		$2B_{2u}(2\Gamma_4^-)$		$2B_2[2B_{2u}(2\Gamma_4^-)]$	[*xz*]
		$2B_{2u}(2Z_4^-)$		$2B_2[2B_{2u}(2Z_4^-)]$	[*xz*]
$7E_u$		$7E_u(7\Gamma_5^-)$		$7A_1[7E_u(7\Gamma_5^-)]$	[*xx,yy,zz*]
				$7B_1[7E_u(7\Gamma_5^-)]$	[*xy*]
		$7E_u(7Z_5^-)$		$7A_1[7E_u(7Z_5^-)]$	[*xx,yy,zz*]
				$7B_1[7E_u(7Z_5^-)]$	[*xy*]
$2E_u$		$2E_u(2\Gamma_5^-)$		$2A_1[2E_u(2\Gamma_5^-)]$	[*xx,yy,zz*]
				$2B_1[2E_u(2\Gamma_5^-)]$	[*xy*]
		$2E_g(2Z_5^+)$	*xz,yz*	$2A_2[2E_g(2Z_5^+)]$	*yz*
				$2B_2[2E_g(2Z_5^+)]$	*xz*

1, X-$2Z$ model hereafter). Note that in Table II all atomic coordinates in approximate structures are given in units of corresponding primitive translations.

The GTA of phonon symmetry and Raman selection rules of the two approximate structures are presented in Table III. For the ''X-Z'' structure, the set of optical modes at the Γ point is

$$\Gamma_{\text{opt}} = 3\Gamma_1^+ + \Gamma_2^+ + 4\Gamma_5^+ + 6\Gamma_3^- + 2\Gamma_4^- + 8\Gamma_5^- = 3A_{1g} + B_{1g} + 4E_g + 6A_{2u} + 2B_{2u} + 8E_u, \quad (2)$$

while for the ''X-$2Z$'' structure

$$\Gamma_{\text{opt}} = 8\Gamma_1^+ + 2\Gamma_2^+ + 10\Gamma_5^+ + 11\Gamma_3^- + 4\Gamma_4^- + 15\Gamma_5^- = 8A_{1g} + 2B_{1g} + 10E_g + 11A_{2u} + 4B_{2u} + 15E_u. \quad (3)$$

Hence, the number of A_{1g} modes in the X-Z structure is predicted to be 3, which is clearly less than the observed line number. The second approximation, X-$2Z$ structure, seems to be more appropriate to describe the observed spectra. For this model, three of A_{1g} modes originate from the Γ_1^+ modes of the X-Z structure (see Table III). The remaining modes originate from the Z_1^+ modes of the X-Z structure projected into the Γ point when increasing the primitive cell along the z direction in the X-$2Z$ structure. We can expect that A_{1g} modes associated with the NdI/NdII, CuIII/CuIV, and O_{CuII}/O_{CuIV} atom pairs exhibit no essential frequency split to be resolved in the Raman spectra. In other words, only three corresponding lines could be observed in the *zz* polarization. The other two A_{1g} modes, which are absent in the simplest X-Z structure, are induced by vibrations of Ba and O_{Ba} atoms. The two A_{1g} Raman-active modes in the X-$2Z$ struc-

ture originate from $2Z_1^+$ modes in the X-Z structure that are folded into the Γ point. Thus, in the case of the X-$2Z$ model, five lines are expected in the zz polarization.

We propose the following assignment of these 5 lines: ν_1(Ba)=134 cm^{-1}, ν_3(CuIII,CuIV)=158 cm^{-1}, ν_4(NdI,NdII) =269 cm^{-1}, $\nu_7(O_{CuIII}\,O_{CuIV})$=440 cm^{-1}, $\nu_9(O_{Ba})$=548 cm^{-1}. It is based on the Raman data of parent compounds $Nd_{1+x}Ba_{2-x}Cu_3O_y$ and Nd_2CuO_4, taking into account changes of interatomic distances. Note that the extra line ν_{10} at 579 cm^{-1} in the zz polarization originates from the residual oxygen disorder in CuO_2 layers in the ''imperfect'' $Nd_2Ba_1Cu_3O_7$ structure. Since the increase of x does not affect the arrangement around the CuO_2 layers (Cu=CuIII, CuIV) (Refs. 7 and 11 and Table II), we expect no essential changes of frequency of A_g modes involving atoms in the CuO_2 layers (ν_3, ν_7) for the transformation from $NdBa_2Cu_3O_y$ to $Nd_2Ba_1Cu_3O_y$. On the contrary, the frequency of A_g modes involving the BaO layer (ν_1, ν_9) is expected to increase owing to the substitution in the BaO layer followed by a large decrease of the c-lattice constant (about 0.4 Å). Indeed, frequencies of A_g modes involving the CuO_2 layers are ν_3=153 cm^{-1}, ν_7=430 cm^{-1} for the $NdBa_2Cu_3O_y$ crystal and ν_3=158 cm^{-1}, ν_7=440 cm^{-1} for the $Nd_{1.85}Ba_{1.15}Cu_3O_y$ crystal (see Table I). In contrast, frequencies of the A_g modes of BaO layer atoms in $NdBa_2Cu_3O_y$ (ν_1=119 cm^{-1} and ν_9=514 cm^{-1}) are noticeably smaller than that in the x=0.85 crystal (ν_1 =134 cm^{-1} and ν_9=548 cm^{-1}).

The A_g mode of NdI and NdII atoms is associated with the remaining lines (ν_4=269 cm^{-1}), although the crystal-field phonon-coupling effect might not be excluded.[26] It is reasonable that the ν_4 line is absent in the RSS of the $NdBa_2Cu_3O_y$ crystal (Fig. 2) because vibrations of Nd atoms at sites with inversion are active only in infrared spectra.[12,13] It should be noted that the frequency of the Nd vibration is about 230 cm^{-1} in the Nd_2CuO_4 structure.[27] A slight increase of this frequency for the $Nd_{1.85}Ba_{1.15}Cu_3O_y$ compound can be naturally explained by different distances between nearest Nd layers (about 3.65 and 3.58 Å for Nd_2CuO_4 and $Nd_{1.9}Ba_{1.1}Cu_3O_y$, respectively). The width of the 269-cm^{-1} line (about 50 cm^{-1}) in the $Nd_{1.85}Ba_{1.15}Cu_3O_y$ crystal is several times larger than that of the 230-cm^{-1} line in Nd_2CuO_4 [less than 10 cm^{-1} (Ref. 27)]. There are two reasons for such broadening in the $Nd_{1.85}Ba_{1.15}Cu_3O_y$ compound. The first is disorder in the Nd sublattice and the second is a possible splitting of the A_g mode as predicted by GTA for the X-$2Z$ structure (Table III). Note that the insertion of Ce atoms also results in additional broadening of this line (linewidth about 20 cm^{-1}) in $Nd_{1.85}Ce_{0.15}CuO_4$.[28]

As for the xx, $x'y'$, and $x'x'$ polarizations, the 296-cm^{-1} line can be assigned to the B_{1g} vibration (ν_5), because it is detected in the xx, yy, $x'y'$ polarizations but completely disappears in the $x'x'$, $y'y'$, and zz polarizations as is typical for the B_{1g} modes in perovskitelike high-temperature superconductors.[12,13] According to the GTA results, there are two B_{1g} modes induced by O_{CuIII} and O_{CuIV} atoms in the X-$2Z$ structure. However, one can expect that the frequency splitting of these two B_{1g} modes is small, which results in a line broadening only ($\Delta\nu_5 \approx 40$ cm^{-1} in comparison with 30 cm^{-1} for $NdBa_2Cu_3O_y$).

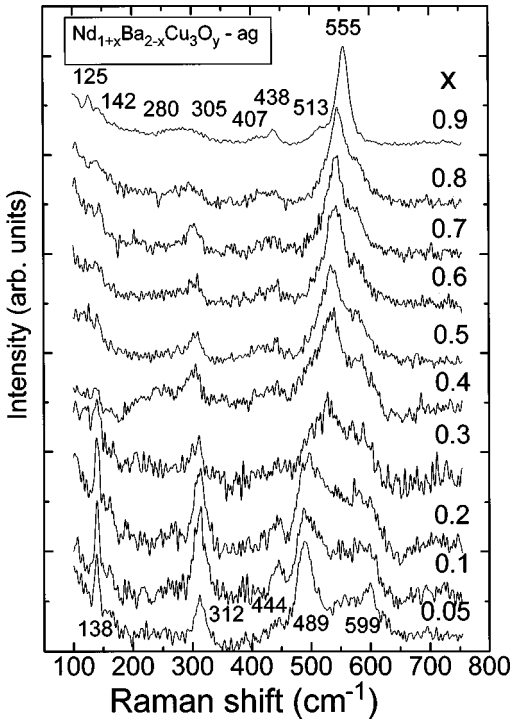

FIG. 3. Raman spectra of as-grown $Nd_{1+x}Ba_{2-x}Cu_3O_y$ solid solutions with different x values at the room temperature (intensities are normalized using the intensity of the A_g apical oxygen line).

The two low-frequency lines at 120 cm^{-1} (ν_1) and 144 cm^{-1} (ν_2) can be associated with the A_g vibrations of heavy atoms (Ba, Cu, and Nd), whereas the two high-frequency lines at 438 cm^{-1} (ν_7) and 546 cm^{-1} (ν_9) are related to the

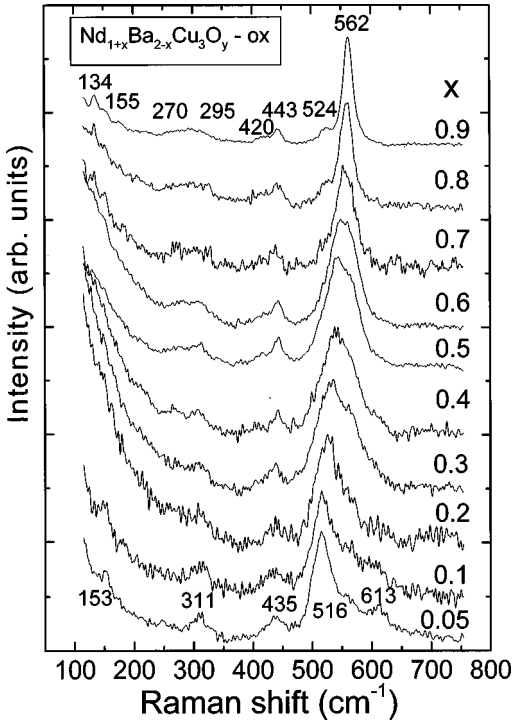

FIG. 4. Raman spectra of oxygenated $Nd_{1+x}Ba_{2-x}Cu_3O_y$ solid solutions with different x values at the room temperature (intensities are normalized using the intensity of the A_g apical oxygen line).

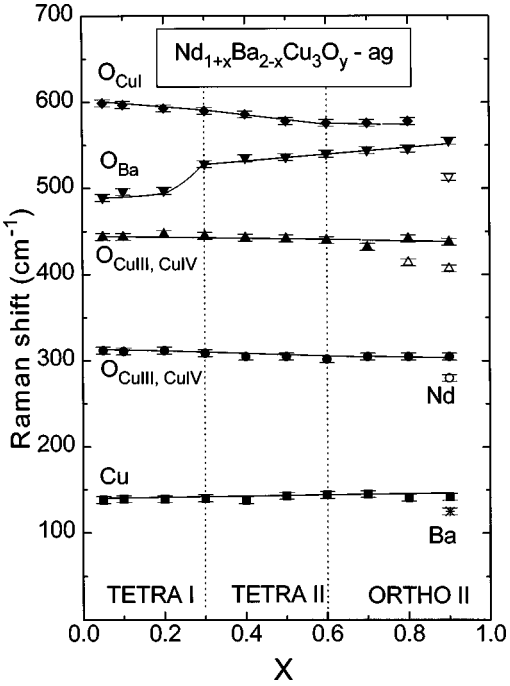

FIG. 5. Concentrational (x) dependence of Raman frequencies of as-grown $Nd_{1+x}Ba_{2-x}Cu_3O_y$ solid solutions at the room temperature.

A_{1g} modes of O_{CuIII}/O_{CuIV} and O_{Ba} atoms, respectively. A number of additional weak lines such as the 230-cm^{-1} line for the $Nd_{1.85}Ba_{1.15}Cu_3O_y$ crystal in the xx and yy polarizations and the 420-cm^{-1} (ν_6) and 524-cm^{-1} (ν_8) lines in ceramics $Nd_{1.9}Ba_{1.1}Cu_3O_7$ can be connected with other vibration modes in $Nd_2Ba_1Cu_3O_7$ since the complete set of Raman-active modes includes $8A_{1g}+2B_{1g}+10E_g$ vibrations.

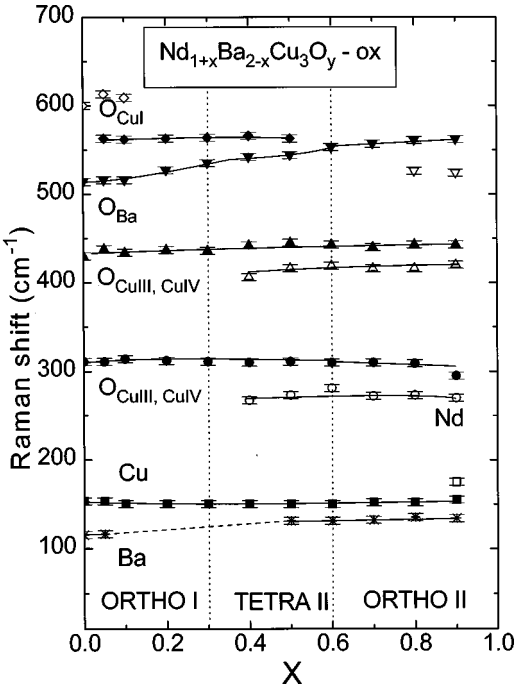

FIG. 6. Concentrational (x) dependence of Raman frequencies of oxygenated $Nd_{1+x}Ba_{2-x}Cu_3O_y$ ($y\approx 7$) solid solutions at the room temperature.

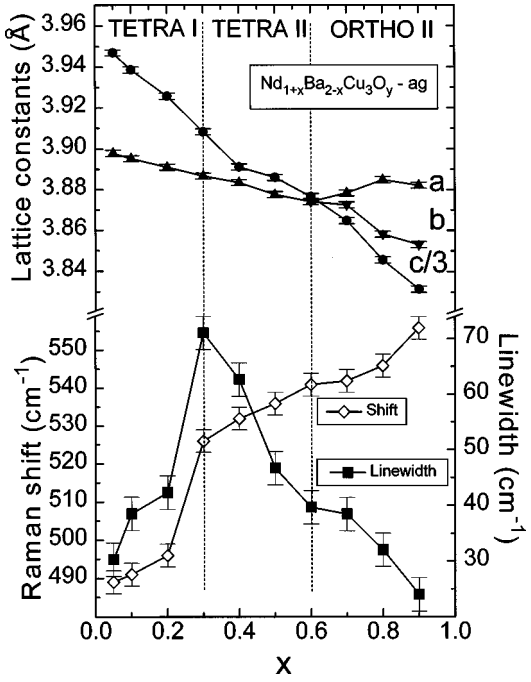

FIG. 7. Concentrational (x) dependencies of $a(a_{sub})$, b, $c(c_{sub})$ lattice constants, frequency $\nu_9(x)$, and linewidth $\gamma_9(x)$ for as-grown $Nd_{1+x}Ba_{2-x}Cu_3O_y$ solid solutions.

Finally, we show the RSS of both as-synthesized (''as-grown,'' ag) and oxygen-annealed (''oxygenated,'' ox) $Nd_{1+x}Ba_{2-x}Cu_3O_y$ ceramics in Figs. 3 and 4, respectively. Figures 5 and 6 demonstrate the concentrational (x) dependencies of Raman frequencies for the samples. The frequencies of all observed phonon peaks in the $Nd_{1.9}Ba_{1.1}Cu_3O_7$ ox samples are listed in Table I.

To interpret the RSS we classify all the lines into three sets: (i) the lines observed in the whole concentration region $x=0-0.9$, (ii) the lines disappearing with increasing x, and (iii) the new lines appearing with increasing x. The first set includes the ν_3, ν_5, ν_7, and ν_9 lines. These four modes originate from the A_g modes of the $NdBa_2Cu_3O_7$ lattice and their mode assignment is well established (Table I). The fifth A_g mode of the $NdBa_2Cu_3O_7$ lattice ν_1 has lower intensity and vanishes at the intermediate x values due to strong Rayleigh scattering in ceramic samples. The ν_{10} line is classified into the second set. It is induced by the oxygen disorder in the CuO chains and, as a result, the intensity is higher in the RSS of ag samples (see Figs. 3 and 4 for comparison). This line becomes weaker with increase of x and completely disappears at $x=0.9$ in both ag and ox samples, probably as a consequence of absence of the CuO chain in the $Nd_2Ba_1Cu_3O_7$ structure. The ν_2, ν_4, ν_6, and ν_8 lines belong to the third set of lines, as discussed above.

B. Concentration-dependent phase transformations in the $Nd_{1+x}Ba_{2-x}Cu_3O_y$ solid solution

The $NdBa_2Cu_3O_y$ lattice undergoes structural transformations upon the substitution of Nd^{3+} (1.11 Å) for Ba^{2+} (1.35 Å). First of all, the substitution gives rise to a nonmonotonous reducing a-, b-, and c-lattice constants (Figs. 7 and 8). Basing on these XRD results, we can divide the x range into three regions. In the first of them ($0\leqslant x\leqslant 0.3$) the ag

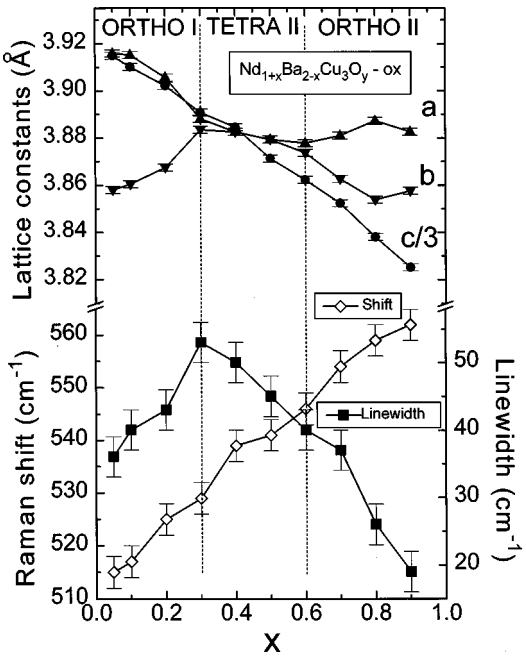

FIG. 8. Concentrational (x) dependencies of $a(a_{\mathrm{sub}})$, b, $c(c_{\mathrm{sub}})$ lattice constants, frequency $\nu_9(x)$, and linewidth $\gamma_9(x)$ for oxygenated $Nd_{1+x}Ba_{2-x}Cu_3O_y$ solid solutions.

samples are tetragonal ($a=b<c/3$, TETRA I). As the oxygen content increases, a phase transition takes place from the tetragonal to the orthorhombic structure (ORTHO I). In the second region ($0.3\leqslant x\leqslant 0.6$), both ag and ox samples of the $Nd_{1+x}Ba_{2-x}Cu_3O_y$ solid solution are tetragonal with $a=b\approx c/3$ (TETRA II).[3–6] Finally, in the third region ($0.6\leqslant x\leqslant 0.9$), both ag and ox samples become orthorhombic (ORTHO II) with a superstructure imposed along the x and z axes with periods $a=2a_{\mathrm{sub}}$, $b=b_{\mathrm{sub}}$, and $c=2c_{\mathrm{sub}}$. In this section, we determine features of the structural phase transitions between $x=0$ and $x=1$ regarding their effect on RSS.

First we discuss the changes in Raman spectra and XRD at $x\approx 0.3$. Among all the phonon modes the ν_9 apical-oxygen mode was found to be very sensitive to the structural changes. In Figs. 7 and 8 we plot the concentrational dependencies of the frequency $\nu_9(x)$ and the linewidth $\gamma_9(x)$ for ag and ox samples together with the $a(a_{\mathrm{sub}})$, b, $c(c_{\mathrm{sub}})$ lattice constants. Oxygenated samples exhibit a direct correlation between Raman and XRD data corresponding to the ORTHO I–TETRA II structural transition. According to XRD data, the a and b lattice constants become equal at $x\approx 0.3$ while the phonon linewidth $\gamma_9(x)$ shows a pronounced maximum. Note that at the same composition the oxygenated solid solution becomes completely nonsuperconducting.[4,5] More dramatic change can be observed in the Raman spectra rather than in the XRD patterns for the ag samples. The frequency $\nu_9(x)$ jumps about 30 cm^{-1} between $x=0.2$ and 0.3, and the transition is accompanied by a pronounced maximum of the line broadening at $x\approx 0.3$.

Segre *et al.*[29] suggested that oxygen disorder in the basal plane caused by the rare-earth element doping has a direct relationship with T_c for a solid solution such as $Nd_{1+x}Ba_{2-x}Cu_3O_y$. Later the charge-transfer theories have been applied as well.[3–6] From our results, oxygen disordering can be observed in RSS upon the transition into the TETRA II phase at $x\approx 0.3$. The XRD is insensitive to the change of oxygen distribution, unless the structure symmetry changes. Therefore, XRD shows no clear change at $x=0.3$ in the ag samples. In RSS, the ν_9 mode is determined mainly by force constants between the apical oxygen and two neighboring Cu. Consequently, the oxygen disorder has to result in local fluctuations of the force constants in this and neighboring layers and it leads to the maximum of the ν_9 linewidth. Additionally, existence of the disordered oxygen in the basal plane eliminates the difference between the a and b axis, i.e., results in disappearing the orthorhombicity at $x=0.3$ for XRD measurements. It is impossible to keep highly ordered -O-Cu-O- chains and unoccupied vacancy chains if Nd at Ba sites requires oxygen atoms to be entered occasionally into the vacancies.[3] In other words, the structural transition around $x=0.3$ is caused by the oxygen disordering in the $NdBa_2Cu_3O_y$ unit cell with a random distribution of extra Nd.

In contrast, the TETRA II–ORTHO II phase transition at $x\approx 0.6$ has a different nature. Although the XRD clearly shows the orthorhombic splitting at $x>0.6$ ($a_{\mathrm{sub}}\neq b_{\mathrm{sub}}$), there is no significant anomaly in x dependence of the main oxygen modes ν_5, ν_7, ν_9. Since the ν_{10} vibration, related to the oxygen disorder in the $CuO_{1+\delta}$ layer, is clearly observed till $x=0.8$, it is deduced that oxygen is not primarily responsible for this phase transition. Moreover, it should be noted that the $Nd_{1.9}Ba_{1.1}Cu_3O_y$ phase is orthorhombic even at 1000 °C in air.[10] In the case that distribution of Nd and Ba in the structure is random, especially under the condition of high oxygen mobility at elevated temperatures, no possibility for the $Nd_2Ba_1Cu_3O_y$ phase to demonstrate the orthorhombicity can be assumed.

It is expected that the unit cell is compressed by the Ba substitution with smaller Nd ions. Indeed, the lattice constants decrease and phonon mode frequencies increase with increasing x (Figs. 5–8). According to the lattice-dynamics considerations[30] such a ''chemical compression'' can reduce stiffness of transverse motions of atoms in linear or planar polyatomic fragments of the crystal lattice. The effect originates from the pressure-induced internal tensions[31] that lead to anharmonicity of vibrations and at some critical values it may result in the lattice instability and structural transitions.[32] In the $Nd_{1+x}Ba_{2-x}Cu_3O_y$ solid solution, a new type of heavy-atom ordering becomes stable at the large substitution $x>0.6$, leading to the TETRA II–ORTHO II phase transition and the $Nd_2Ba_1Cu_3O_y$ structure, which is described above. It determines a new type of oxygen ordering as well, and the phonon linewidth $\gamma_9(x)$ falls down to its minimum value.

IV. CONCLUSIONS

The Raman scattering spectra of $Nd_{1+x}Ba_{2-x}Cu_3O_y$ compounds within the range $0\leqslant x\leqslant 0.9$ were studied. The polarized RSS of detwinned $NdBa_2Cu_3O_y$ single crystal as well as twinned Nd-rich $Nd_{1.85}Ba_{1.15}Cu_3O_y$ crystals and solid solutions with $x>0.6$ were investigated for the first time and all main phonon lines were assigned. To interpret the RSS, we have performed a GTA for the exact and two approximate structures of the $Nd_2Ba_1Cu_3O_7$ lattice. It is seen that the number of the observed phonon lines is smaller than that

predicted for the exact $2X$-$2Z$ structure. We have established that the observed RSS of the $Nd_{1.85}Ba_{1.15}Cu_3O_y$ single crystal are well described in the framework of the approximate X-$2Z$ structure. It indicates that the distortion of the X-Z structure leading to doubling of the sublattice parameter c is an essential structural transformation and that it is directly reflected in phonon spectra.

The concentrational (x) behavior of the phonon lines in RSS is consistent with the picture of two structural transitions at $x \approx 0.3$ and $x \approx 0.6$ observed by XRD. The first one at $x \approx 0.3$ is connected with a reconstruction of the oxygen sublattice: the oxygen disorder results in broadening and nonmonotonous behavior of the ν_9 apical oxygen mode. Such noticeable anomalies in the oxygen mode behavior are absent at the second phase transition at $x \approx 0.6$. It suggests that heavy atoms play an important role in this TETRA II–ORTHO II phase transition; particularly, the lattice distortion is due to the internal ''chemical pressure'' induced by the substitution of smaller Nd^{3+} for Ba^{2+}.

ACKNOWLEDGMENTS

The authors are grateful to A. G. Panfilov for fruitful critical discussions and K. Tomimoto for detwinning of the $NdBa_2Cu_3O_y$ crystal. This work was supported by the New Energy and Industrial Technology Development Organization for R&D of the Industrial Science and Technology Frontier Program.

*Permanent address: A. F. Ioffe Physical-Technical Institute, 194021 St. Petersburg, Russia.

[1] M. Murakami, S. I. Yoo, and T. Higuchi, Jpn. J. Appl. Phys., Part 2 **33**, L715 (1994).

[2] M. Nakamura, Y. Yamada, T. Hirayama, Y. Ikuhara, Y. Shiohara, and S. Tanaka, Physica C **259**, 295 (1996).

[3] M. J. Kramer, S. I. Yoo, R. W. McCallum, W. B. Yelon, H. Xie, and P. Allenspach, Physica C **219**, 145 (1994).

[4] S. Li, A. Hayri, and K. V. Ramanujachary, Phys. Rev. B **38**, 2450 (1988).

[5] D. V. Fomichev, O. G. D'yachenko, A. V. Mironov, and E. V. Antipov, Physica C **225**, 25 (1994).

[6] M. J. Kramer, A. Karion, and K. W. Dennis, J. Electron. Mater. **23**, 1117 (1994).

[7] E. A. Goodilin, N. N. Oleynikov, G. Yu. Popov, V. A. Shpanchenko, E. V. Antipov, G. V. Balakirev, and Yu. D. Tretyakov, Physica C **272**, 65 (1996).

[8] K. Osamura and W. Zhang, Z. Metallkd. **84**, 522 (1993).

[9] E. Goodilin, M. Kambara, T. Umeda, and Y. Shiohara, Physica C **289**, 251 (1997).

[10] E. A. Goodilin, A. Oka, J. G. Wen, Y. Shiohara, M. Kambara, and T. Umeda, Physica C **299**, 279 (1998).

[11] N. Khasanova, E. Goodilin, X. Wu, S. Tajima, and Y. Shiohara (unpublished).

[12] C. Thomsen, in *Light Scattering in Solids VI*, edited by M. Cardona and G. Guntherodt (Springer, Berlin, 1991), p. 285.

[13] Yu. E. Kitaev, M. F. Limonov, A. P. Mirgorodsky, A. G. Panfilov, and R. A. Evarestov, Fiz. Tverd. Tela (St. Petersburg) **36**, 865 (1994) [Phys. Solid State **36**, 475 (1994)].

[14] Y. Morioka, M. Kikuchi, and Y. Syono, Jpn. J. Appl. Phys., Part 2 **26**, L1499 (1987); M. Cardona, R. Liu, C. Thomsen, M. Bauer, L. Genzel, W. Konig, and A. Wittlin, Solid State Commun. **65**, 71 (1988); R. Nishitani, N. Yoshida, Y. Sasaki, and Y. Nishina, Jpn. J. Appl. Phys., Part 2 **28**, L569 (1989).

[15] M. Yoshida, S. Gotoh, T. Takata, N. Koshizuka, and S. Tanaka, Phys. Rev. B **41**, 11 689 (1990).

[16] K. F. McCarty, J. Z. Liu, R. N. Shelton, and H. B. Radousky, Phys. Rev. B **41**, 8792 (1990).

[17] M. F. Limonov, A. I. Rykov, and S. Tajima, Physica C **282-287**, 1029 (1997); M. F. Limonov, A. I. Rykov, S. Tajima, and A. Yamanaka, Phys. Rev. Lett. **80**, 825 (1998).

[18] E. Goodilin, M. Kambara, T. Umeda, and Y. Shiohara, Physica C **289**, 37 (1997).

[19] R. A. Evarestov and V. P. Smirnov, in *Site Symmetry in Crystals: Theory and Applications*, edited by M. Cardona, Springer Series in Solid State Sciences Vol. 108 (Springer, Heidelberg, 1993).

[20] Yu. E. Kitaev, A. G. Panfilov, P. Tronc, and R. A. Evarestov, J. Phys.: Condens. Matter **9**, 257 (1997); **9**, 277 (1997).

[21] Yu. E. Kitaev, M. F. Limonov, A. G. Panfilov, R. A. Evarestov, and A. P. Mirgorodsky, Phys. Rev. B **49**, 9933 (1994).

[22] A. A. Bush, Yu. E. Kitaev, M. F. Limonov, Yu. F. Markov, A. A. Novikov, and R. A. Evarestov, Physica C **190**, 477 (1992).

[23] E. Goodilin, M. Limonov, A. Panfilov, N. Khasanova, A. Oka, S. Tajima, and Y. Shiohara, Physica C **300**, 250 (1998).

[24] X. Yao and Y. Shiohara, Supercond. Sci. Technol. **10**, 249 (1997).

[25] H. Schmid, E. Burkhardt, B. N. Sun, and J. P. Rivera, Physica C **157**, 555 (1989).

[26] T. Ruf, E. T. Heyen, M. Cardona, J. Mesot, and A. Furrer, Phys. Rev. B **46**, 11 792 (1992).

[27] S. Jandl, M. Iliev, C. Thomsen, T. Ruf, and M. Cardona, Solid State Commun. **87**, 609 (1993).

[28] E. T. Heyen, G. Kliche, W. Kress, W. Koning, and M. Cardona, Solid State Commun. **74**, 1299 (1990).

[29] C. U. Segre, B. Dabrowski, D. G. Hinks, K. Zhang, and J. D. Jorgensen, Nature (London) **329**, 227 (1987).

[30] A. P. Mirgorodsky and M. B. Smirnov, J. Phys.: Condens. Matter **5**, 3313 (1993).

[31] A. P. Mirgorodsky, M. B. Smirnov, P. E. Quintard, and T. Merle-Mejean, Phys. Rev. B **52**, 9111 (1995).

[32] O. H. Nielsen and R. M. Martin, Phys. Rev. B **32**, 3780 (1985).